Invariant cross section for the inclusive reaction $p + p \rightarrow p + X$ at 205 GeV/c

J. Whitmore*
Fermi National Accelerator Laboratory, Batavia, Illinois 60510†

S. J. Barish, D. C. Colley‡, and P. F. Schultz
Argonne National Laboratory, Argonne, Illinois 60439 §

(Received 18 November 1974)

Inclusive proton production in pp interactions at 205 GeV/c is studied using the Fermi National Accelerator Laboratory (Fermilab) 30-in. bubble chamber. The invariant cross section is presented in terms of several kinematic variables and compared with similar data obtained from counter experiments at Fermilab and at the CERN Intersecting Storage Rings (ISR). An important feature of this experiment is that it provides data for much wider ranges of the four-momentum transfer than have been attained in the counter experiments. It also gives full information on the associated charged-particle multiplicity of every event, thus permitting a detailed investigation of how various kinematic quantities depend on this parameter.

I. INTRODUCTION

Recent measurements of the invariant cross section for the inelastic inclusive reaction

$$p + p \rightarrow p + X \tag{1}$$

have generated a great deal of interest, both theoretically and experimentally, in terms of the dependence of this process on both the charged multiplicity of X and the kinematic variables of the recoil proton. A counter experiment[1] at the CERN Intersecting Storage Rings (ISR) (at center-of-mass energy squared $s = 930$ GeV^2 and $s = 1995$ GeV^2) has reported results on reaction (1) for values of p_T, the transverse momentum of the outgoing proton, greater than $\simeq 0.5$ GeV/c. At the Fermi National Accelerator Laboratory (Fermilab), this reaction has been studied in one counter experiment[2] for $100 < s < 750$ GeV^2 in the region $-0.38 < t < -0.14$ (GeV/c)^2, where t is the square of the four-momentum transferred from the target to the recoil proton. A second counter experiment[3] at Fermilab has obtained data at 300 GeV/c incident proton momentum in the range $-0.19 < t < -0.019$ (GeV/c)^2. The 102 and 303 GeV/c bubble-chamber experiments[4,5] at Fermilab have provided some data on the multiplicity dependence and on the behavior at small p_T. The experiment reported here, the study of 205 GeV/c ($s = 386$ GeV^2) proton-proton interactions, provides additional data in this very important low p_T region where most of the events of reaction (1) occur. A study of the distributions of the square of the missing mass, M^2, recoiling from the slow proton and some characteristics of the t and multiplicity dependence of reaction (1) determined from this experiment have already been published.[6,7] In this paper we give new and more detailed information on the behavior of the invariant cross section as a function of p_T, of t, and of the Feynman variable $x = p_L^*/p_{\max}^* \simeq 2p_L^*/\sqrt{s}$ (p_L^* is the longitudinal momentum of the recoil proton in the c.m. system and $p_{\max}^*$ is the momentum of the incoming protons in the c.m. system). We also present further analysis of the charged multiplicity dependence of reaction (1) with comparisons to the multiplicity dependence of the reaction

$$p + p \rightarrow n \text{ charged particles} + X\,. \tag{2}$$

II. EXPERIMENTAL DETAILS

The experiment reported here was carried out using the 30-in. hydrogen bubble chamber exposed to a beam of 205-GeV/c protons at the Fermi National Accelerator Laboratory. Within a selected fiducial volume, 8810 events[8] were examined visually in a search for protons that could be identified by bubble density. Candidate tracks were measured on POLLY III at Argonne National Laboratory and spatially reconstructed using TVGP with a 98.5% passing rate. The remaining 1.5% do not represent any significant bias regarding the results presented here. The successful events were then looked at by physicists to see if the observed bubble density of each track was consistent with that expected for a proton; 3606 tracks due to protons with laboratory momentum less than 1.4 GeV/c were identified in this manner. Kinematic quantities for each event were computed using the measured information for the recoil proton and the dip and azimuth for the beam

obtained by averaging measurements on full-length beam tracks. The momentum of the beam was fixed at 205 ± 2 GeV/c. The resolution in M^2, estimated using the beam parameters and the errors on the measured momentum and direction of the slow proton, is ± 1.5 GeV^2 at low M^2 and increases to $\sim \pm 2$ GeV^2 at $M^2 = 200$ GeV^2 [where $M^2 \simeq s(1+x)$ for $M^2 \ll s$]. This corresponds to a resolution $\delta x = \pm 0.004$ near $x = -1$. Topology dependent corrections for scanning and processing losses were computed from a rescan of part of the film for slow proton candidates and from a study of events failing TVGP after two measurement passes. These correction factors range from 1.02 for two-prongs to 1.13 for events with ten or more prongs.

To display the kinematic region in which we study reaction (1), we show in Fig. 1 a scatter plot of x, the Feynman variable, versus p_T, the transverse momentum of the recoil proton. The highly populated band near $x = -1$ is dominated by the elastic events which have not been removed from this figure. The curved boundary caused by the 1.4 GeV/c laboratory momentum cut shows that this selection of protons results in no significant experimental biases for $x < -0.7$, corresponding to $M^2 \lesssim 120$ GeV^2. For small p_T (e.g., $p_T \lesssim 400$ MeV/c), we can obtain an unbiased distribution for $x \lesssim -0.4$.

To obtain the distributions for the inelastic events, the elastic events which form the majority of the two-prong events have been subtracted. All two-prong events in the exposure have been measured completely and kinematically fitted. Events that give an elastic fit or that have not been measured well enough for a 3- or 4-constraint kinematic fit to be attempted have been removed from our sample.[9] Each of the remaining (inelastic) two-prongs is given a weight of 1.15 to correct for the events for which no fit could be attempted.

Very slow protons in the two- and four-prong events cannot always be seen in the chamber if they are steeply dipping and have $0.10 \lesssim p_{\text{lab}} \lesssim 0.14$ GeV/c. Furthermore, for $p_{\text{lab}} \lesssim 0.10$ GeV/c, protons often cannot be observed at all. For the inelastic two-prongs, we estimate that 16 events are lost and for the four-prongs, that seven are lost (these were recorded in scanning as three-prongs), so appropriate weights are used to compensate for these losses. We emphasize that because of a lack of knowledge of the shape of $d\sigma/dt$ for inelastic two-prongs at very small t we have not corrected the inelastic two-prong sample for a possible loss of events with protons too short to be seen at any dip angle, so our data at low t near $x = -1$ represent a lower limit for the cross section in this region.

Table I shows the raw number of inelastic events,

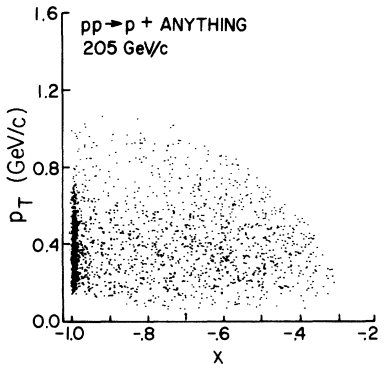

FIG. 1. Scatter plot of p_T versus x for the reaction $p + p \to p + X$ at 205 GeV/c. Note that the elastic events have not been removed from this plot.

as a function of topology, that have an identified proton with laboratory momentum less than 1.4 GeV/c. In this experiment, the normalization is obtained[8] by equating the total number of interactions to a pp total cross section of $\sigma_T = 39.0 \pm 1.0$ mb and should be accurate to $\pm 3\%$. Using the resulting (4.35 ± 0.14) μb/event, we obtain the inelastic cross sections for observing a proton with $p_{\text{lab}} < 1.4$ GeV/c. These cross sections are also given in Table I where the quoted values include both the corrections made for any uncertainties in proton identification as well as the $\pm 3\%$ overall normalization uncertainty.

III. INVARIANT CROSS SECTION

The invariant cross section may be presented in several ways, depending upon the variables that are used. The following expressions will be used

TABLE I. Topological cross sections for $p + p \to p + X$, with $p_{\text{lab}}(p) < 1.4$ GeV/c.

Topology	Raw number of events	Cross section (mb)
2 (inelastic)	300	1.62 ± 0.22
4	680	3.13 ± 0.14
6	570	2.65 ± 0.13
8	398	1.90 ± 0.10
10	239	1.17 ± 0.08
12	109	0.54 ± 0.05
14	38	0.19 ± 0.03
16	20	0.098 ± 0.022
18	5	0.025 ± 0.012
20	1	0.005 ± 0.005
Total	2360	11.33 ± 0.33

in this paper:

$$f(\vec{p}, s) = E\frac{d^3\sigma}{dp^3} \xrightarrow[s\to\infty]{} \frac{2E}{\pi\sqrt{s}}\frac{d^2\sigma}{dx dp_T{}^2} \tag{3}$$

$$\xrightarrow[s\to\infty]{} \frac{s}{\pi}\frac{d^2\sigma}{dt\,dM^2} \tag{4}$$

$$= \frac{2E}{\pi\sqrt{s}}\frac{1}{x}\frac{d^2\sigma}{dt\,dx} \quad , \tag{5}$$

where E is the energy of the recoil proton in the c.m. system.

Values of the invariant cross section, Eq. (3), are given in Tables II and III as a function of x and $p_T{}^2$ and are shown in Fig. 2 versus x for various $p_T{}^2$ ranges and in Fig. 3 versus $p_T{}^2$ for various x ranges. The dominant features of the data are the peak near $x=-1$, produced by target fragmentation, and the relatively flat x distribution for $x \gtrsim -0.9$. We also show in these figures the data of Albrow *et al.*[1] from the ISR and of the 303 GeV/c bubble-chamber experiment.[5] There is good agreement between our results and those from both the ISR and Fermilab experiments. This shows that, in the ranges of $p_T{}^2$ and x where the results overlap, scaling is good to within the accuracy of the data. Our results confirm the finding of Dao *et al.*[5] that the data at low $p_T{}^2$ lie well above a single exponential extrapolation in $p_T{}^2$ of the ISR results.

These data may also be presented in terms of their x dependence for fixed t. The invariant cross section, Eq. (5), is given in Table IV and is shown in Fig. 4 where they are compared with the Fermilab data of Abe *et al.*[2] For the purpose of this comparison, these counter data are represented by the simple parametrization of the form

$$E\frac{d^3\sigma}{dp^3} = A(x)\,e^{b(x)t}\left(1+\frac{B(x)}{\sqrt{s}}\right) \tag{6}$$

for the region $-0.93 < x < -0.80$ and are in good agreement with our data at 205 GeV/c. The dominant feature of Fig. 4 is the dip in the invariant cross section near $x=-0.9$ followed by the rise for larger values of x. It is clear, however, that the dip is present only for $t < -0.1$ (GeV/c)^2. For smaller values of $|t|$ the dip has disappeared, leaving only a hint of a shoulder in the cross section near $x=-0.9$. Furthermore, within the errors, there is no indication that the position of the dip is dependent upon t. A qualitative understanding of the features observed in Fig. 4 may be obtained by considering[10] Fig. 5, which shows contours of constant t on a plot of $p_T{}^2$ versus x where we have used the relation

$$tx = p_T{}^2 + M_p{}^2(1+x)^2 \tag{7}$$

with M_p = proton mass. From this figure one sees that, since the invariant differential cross section $E\,d^3\sigma/dp^3$ is approximately exponential in $p_T{}^2$ for any fixed x (see Fig. 3) and for any given $p_T{}^2$ it is approximately independent of x (for $x \gtrsim -0.9$), for a given region of t [e.g., -0.2 to -0.3 (GeV/c)^2] there will be a large cross section at $x \approx -1$ as well as an enhancement for larger x (e.g., $x \sim -0.6$). Similarly, one sees, again qualitatively, why for $t \approx 0$ there is no strong indication for a dip.

The falloff for $x > -0.85$ for the $0 > t > -0.1$ (GeV/c)^2 region is due to the $t_{\min}$ effect. This is seen more clearly in the Chew-Low plot shown in Fig. 6. Although we have already presented the data in a previous letter,[6] for completeness we present the invariant cross section (4) in Fig. 7 as a function of t for various ranges of M^2. The t dependence of each distribution can be well fitted[6] by an exponential form except for the regions affected by the kinematic boundary at high M^2.

TABLE II. $E\frac{d^3\sigma}{dp^3} = \frac{2E}{\pi\sqrt{s}}\frac{d^2\sigma}{dx dp_T{}^2}$ [mb/(GeV/c)^2] for $p+p \to p+X$.

$p_T{}^2$ [(GeV/c)^2]	$-1.0 < x < -0.9$	$-0.9 < x < -0.8$	$-0.8 < x < -0.7$	$-0.7 < x < -0.6$
0.00, 0.05	61.7 ± 9.5	23.6 ± 3.5	22.2 ± 2.3	16.9 ± 2.0
0.05, 0.10	39.6 ± 9.5	15.6 ± 2.3	14.7 ± 1.9	13.9 ± 1.9
0.10, 0.15	23.1 ± 3.0	11.1 ± 1.7	8.78 ± 1.40	···
0.15, 0.20	16.4 ± 2.6	8.44 ± 1.50	6.67 ± 1.20	···
0.10, 0.20	···	···	···	8.0 ± 0.9
0.20, 0.30	10.0 ± 1.5	4.18 ± 0.70	5.38 ± 0.79	5.15 ± 0.72
0.30, 0.40	5.76 ± 1.00	3.37 ± 0.66	1.97 ± 0.48	2.63 ± 0.52
0.40, 0.50	2.40 ± 0.70	2.46 ± 0.57	1.51 ± 0.42	2.57 ± 0.52
0.50, 0.60	1.92 ± 0.60	···	1.28 ± 0.39	1.14 ± 0.36
0.50, 0.70	···	0.57 ± 0.19	···	···
0.60, 0.80	1.01 ± 0.30	···	0.98 ± 0.24	0.76 ± 0.20
0.70, 0.90	···	1.17 ± 0.28	···	···
0.80, 1.00	0.52 ± 0.20	···	0.51 ± 0.17	···

TABLE III. $E\frac{d^3\sigma}{dp^3} = \frac{2E}{\pi\sqrt{s}}\frac{d^2\sigma}{dx dp_T^2}$ [mb/(GeV/c)^2] for $p + p \to p + X$.

x	$0 < p_T^2 < 0.05$	$0.05 < p_T^2 < 0.15$	$0.15 < p_T^2 < 0.25$	$0.25 < p_T^2 < 0.35$	$0.35 < p_T^2 < 0.45$
−1.00, −0.99	202.8 ± 28.0	95.2 ± 16.0	33.9 ± 7.5	...	...
−0.99, −0.98	119.6 ± 20.0	59.5 ± 9.5	21.5 ± 5.8	...	...
−1.00, −0.98	...	...	...	12.90 ± 3.20	6.31 ± 2.20
−0.98, −0.96	43.2 ± 8.2	36.5 ± 5.2	14.0 ± 3.2	...	...
−0.96, −0.94	46.4 ± 8.6	19.4 ± 4.5	10.1 ± 2.7	...	...
−0.98, −0.94	...	...	...	7.83 ± 2.00	5.67 ± 1.80
−0.94, −0.92	32.0 ± 6.8	14.1 ± 3.2	7.8 ± 2.4	...	...
−0.92, −0.90	28.9 ± 6.3	10.2 ± 2.6	7.4 ± 2.2	...	...
−0.94, −0.90	...	...	...	5.32 ± 1.20	2.79 ± 0.90
−0.90, −0.85	24.0 ± 3.6	15.0 ± 2.0	7.0 ± 1.4	4.83 ± 1.10	2.39 ± 0.90
−0.85, −0.80	23.3 ± 3.5	11.6 ± 1.7	6.16 ± 1.20	3.50 ± 0.94	2.25 ± 0.75
−0.80, −0.75	20.7 ± 3.2	13.1 ± 1.8	5.73 ± 1.10	2.62 ± 0.79	2.64 ± 0.80
−0.75, −0.70	23.7 ± 3.3	10.4 ± 1.5	6.00 ± 1.20	4.92 ± 1.00	0.92 ± 0.46
−0.70, −0.65	17.8 ± 2.7	10.9 ± 1.5	5.17 ± 1.00	6.05 ± 1.10	2.94 ± 0.90
−0.65, −0.60	16.0 ± 2.5	14.5 ± 1.7	3.70 ± 1.10	3.31 ± 0.80	1.35 ± 0.50

These bubble-chamber data may also be integrated over all t. The resulting $d\sigma/dx$ distributions are shown in Fig. 8 along with some lower energy data[11] as well as other Fermilab bubble-chamber data.[4,5] This distribution shows that for $x \approx -1$, the cross section is rising with energy as one might expect if diffraction dissociation, which would predict a constant $d\sigma/dM^2$, is indeed observed for small M^2.[12] It is also apparent from Fig. 8 that the peak position in $d\sigma/dx$ is moving toward $x = -1$ as the incident beam momentum increases from 19 GeV/c to 405 GeV/c. For $x > -0.95$, the cross section appears to be falling as the incident beam momentum increases from 19

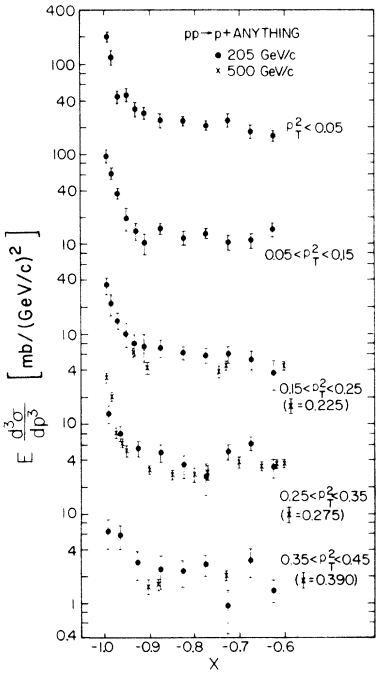

FIG. 2. Invariant cross section as a function of $x = 2p_L^*/\sqrt{s}$ for fixed values of the transverse momentum, p_T (GeV/c).

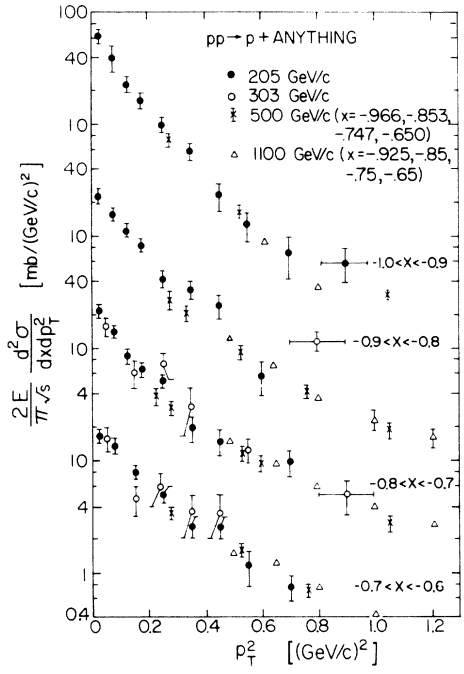

FIG. 3. Invariant cross section as a function of p_T^2 for fixed values of x.

TABLE IV. $E\frac{d^3\sigma}{dp^3} = \frac{2E}{\pi\sqrt{s}}\frac{1}{x}\frac{d^2\sigma}{dtdx}$ [mb/(GeV/c)^2] for $p+p \to p+X$.

x	$0 > t > -0.1$	$-0.1 > t > -0.2$	$-0.2 > t > -0.3$	$-0.3 > t > -0.4$
−1.00, −0.99	162 ± 18	57.3 ± 9.3	•••	•••
−0.99, −0.98	102 ± 12	33.5 ± 7.0	•••	•••
−1.00, −0.98	•••	•••	20.1 ± 4.0	•••
−1.00, −0.96	•••	•••	•••	7.9 ± 1.8
−0.98, −0.96	42.9 ± 6.4	25.5 ± 4.5	•••	•••
−0.96, −0.94	35.6 ± 5.5	14.4 ± 3.4	•••	•••
−0.98, −0.94	•••	•••	8.8 ± 1.7	•••
−0.94, −0.92	23.4 ± 4.1	12.0 ± 3.0	•••	•••
−0.96, −0.92	•••	•••	•••	6.1 ± 1.5
−0.92, −0.90	20.4 ± 4.0	9.0 ± 2.6	•••	•••
−0.94, −0.90	•••	•••	7.2 ± 1.7	•••
−0.90, −0.88	19.7 ± 3.9	11.3 ± 2.9	•••	•••
−0.92, −0.88	•••	•••	•••	6.5 ± 1.6
−0.88, −0.86	21.5 ± 4.0	10.0 ± 2.6	•••	•••
−0.90, −0.86	•••	•••	7.7 ± 1.8	•••
−0.86, −0.84	18.5 ± 3.5	11.5 ± 3.0	•••	•••
−0.88, −0.84	•••	•••	•••	2.3 ± 0.9
−0.86, −0.82	•••	•••	7.8 ± 1.8	•••
−0.84, −0.80	14.6 ± 2.5	12.7 ± 2.6	•••	3.4 ± 1.1
−0.82, −0.78	•••	•••	8.4 ± 1.6	•••
−0.80, −0.76	9.2 ± 1.9	16.2 ± 2.3	•••	5.0 ± 1.4
−0.78, −0.74	•••	•••	5.1 ± 1.3	•••
−0.76, −0.72	6.9 ± 1.4	20.8 ± 2.5	•••	6.6 ± 1.6
−0.74, −0.70	•••	•••	7.3 ± 1.7	•••
−0.72, −0.68	•••	13.5 ± 2.5	•••	8.2 ± 1.8
−0.70, −0.66	•••	•••	13.4 ± 2.4	•••
−0.68, −0.64	•••	8.9 ± 1.9	•••	10.1 ± 2.0
−0.66, −0.62	•••	•••	15.4 ± 2.5	•••
−0.64, −0.60	•••	•••	•••	15.1 ± 2.4
−0.62, −0.58	•••	•••	10.1 ± 2.0	•••
−0.60, −0.56	•••	•••	•••	16.0 ± 2.5
−0.56, −0.52	•••	•••	•••	9.0 ± 1.9

to 102 GeV/c. Within the Fermilab energy region (100–400 GeV/c), the errors on the bubble-chamber data are too large to conclude anything about the energy dependence. It may be noted, however, that the data of Abe *et al.* show[2] that, for fixed x, the invariant cross section is consistent with an $s^{-1/2}$ behavior. These bubble-chamber data do not contradict such a conclusion.[12]

From Fig. 8 we may obtain the average number of protons per inelastic collision at 205 GeV/c. Assuming that the plateau in $d\sigma/dx$ remains constant between -0.6 and 0.6, this integration yields 1.1 ± 0.2 protons/inelastic collision. This is somewhat below the value of 1.41 protons reported by the 19 GeV/c pp experiment,[13] but is consistent with an extrapolation[12] down to 205 GeV/c of the values observed at the ISR.[14]

Figure 9 shows the transverse momentum distribution $d\sigma/dp_T^2$ at 205 GeV/c integrated over the unbiased region of $-1.0 < x < -0.5$. The data appear to be Gaussian in p_T with a change in slope at $p_T^2 \approx 0.2$ (GeV/c)^2. Also shown in Fig. 9 are bubble-chamber data[4] at 102 and 405 GeV/c which show that this distribution has no observable energy dependence when integrated over this region of x.

IV. MULTIPLICITY DEPENDENCE

Reaction (1) may also be studied as a function of the charged-particle multiplicity of the final state. We show in Fig. 10 the missing mass squared distribution $d\sigma/dM^2$ for different charged multiplicities. As previously noted,[6] there is no evidence for a low-mass peak in events with eight or more charged particles in the final state.

Our previous study[6] of the dependence of the charged multiplicity $\langle n_c \rangle$, of the system recoiling off the slow proton in reaction (1), indicated that both the average charged-particle multiplicity,

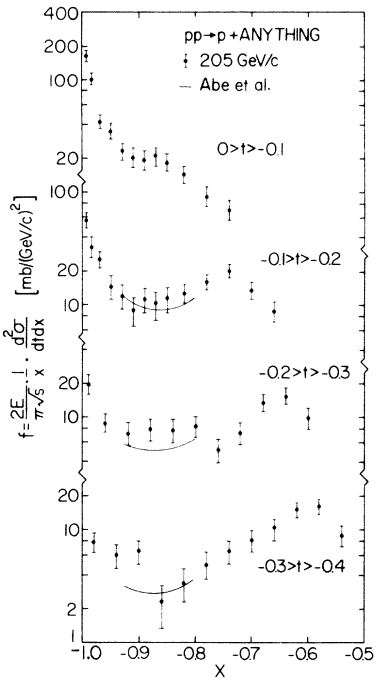

FIG. 4. Invariant cross section as a function of x for fixed values of the four-momentum transfer, t.

$\langle n_c \rangle$, and the second moment, $f_2^{cc} = \langle n_c(n_c-1)\rangle - \langle n_c\rangle^2$, show a very similar energy dependence to the equivalent parameters for the multiplicity distribution observed in reaction (2) when the comparison is made for fixed $s = M^2$. Further studies,[7,15] both on reaction (1) and on the reaction

$$\pi^- + p \to p + X\,, \tag{8}$$

have shown empirically that better agreement is obtained when the comparison is made at fixed available energy. We show in Fig. 11 our values

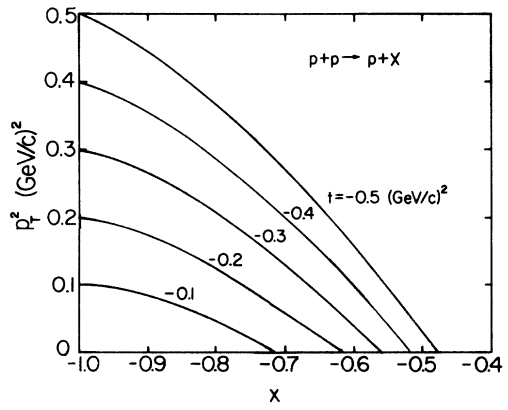

FIG. 5. Plot of $p_T{}^2$ versus x with contours of fixed t.

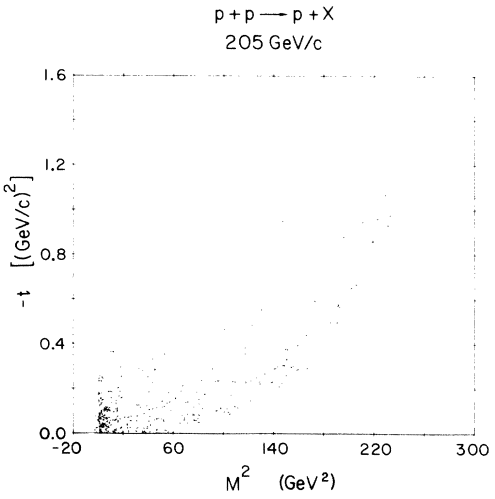

FIG. 6. Chew-Low plot for the reaction $p+p \to p+X$ at 205 GeV/c.

of f_2^{cc} as obtained in reaction (1) as a function of M^2. Recent data[16] from the 102 and 405 GeV/c experiments are also presented in this figure. The solid curve represents f_2^{cc} as obtained from other experiments studying reaction (2) at fixed $s = M^2$. We observe a similar dependence on energy even as low as $s = 10$ GeV^2 (corresponding to $p_{\rm lab} \sim 6$ GeV/c), although the values of f_2^{cc} from the slow proton data do lie systematically above the solid

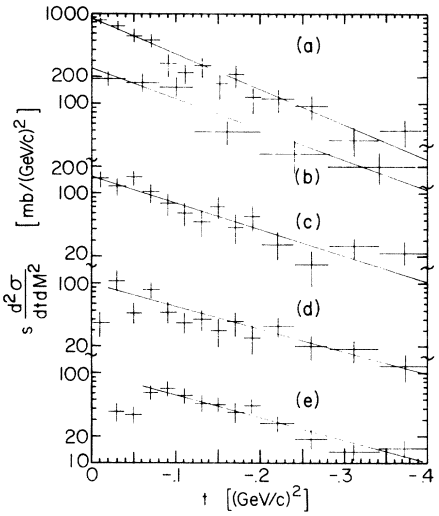

FIG. 7. Invariant cross section versus t for various ranges of missing mass squared. The lines are the results of fits to the form $A\exp(bt)$: (a) $M^2 < 5$ GeV^2, $b = 9.1 \pm 0.7$ (GeV/c)$^{-2}$; (b) $5 \le M^2 < 10$ GeV^2, $b = 8.0 \pm 1.1$ (GeV/c)$^{-2}$; (c) $10 \le M^2 < 25$ GeV^2, $b = 6.1 \pm 0.7$ (GeV/c)$^{-2}$; (d) $25 \le M^2 < 50$ GeV^2, $b = 5.8 \pm 0.7$ (GeV/c)$^{-2}$; (e) $50 \le M^2 < 100$ GeV^2, $b = 5.8 \pm 0.6$ (GeV/c)$^{-2}$.

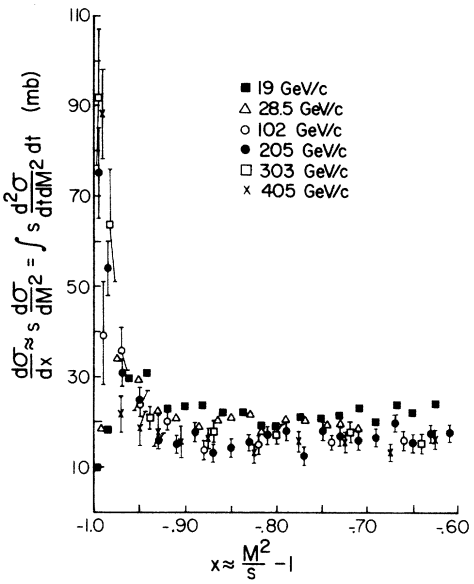

FIG. 8. Inclusive proton differential cross section as a function of x after integration over all p_T^2 (Ref. 12).

curve. Note that for reaction (2), the value of f_2^{cc} must approach $f_2^{cc} = -2$ as $s \to 0$ (below the threshold for two-pion production), whereas f_2^{cc} for reaction (1) appears to approach $f_2^{cc} = -1$.

We now discuss the multiplicity dependence of reaction (1) upon the kinematic variables t and p_T^2 of the recoil proton. Figure 12 shows the average charged multiplicity $\langle n_c \rangle$ as a function of M^2 for three different regions of t. The solid curve in each case represents the overall M^2 dependence

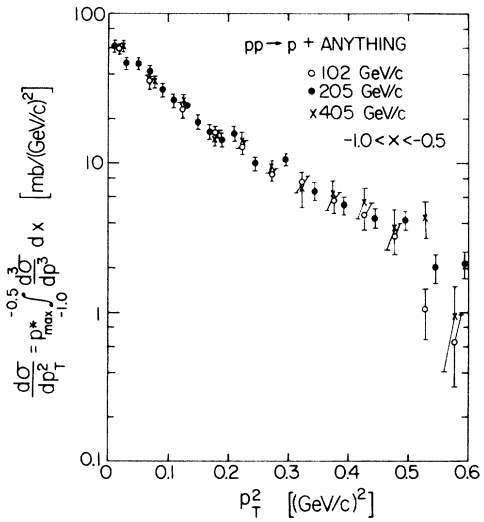

FIG. 9. Inclusive proton differential cross section as a function of p_T^2 for $-1.0 < x < -0.5$ (Ref. 12).

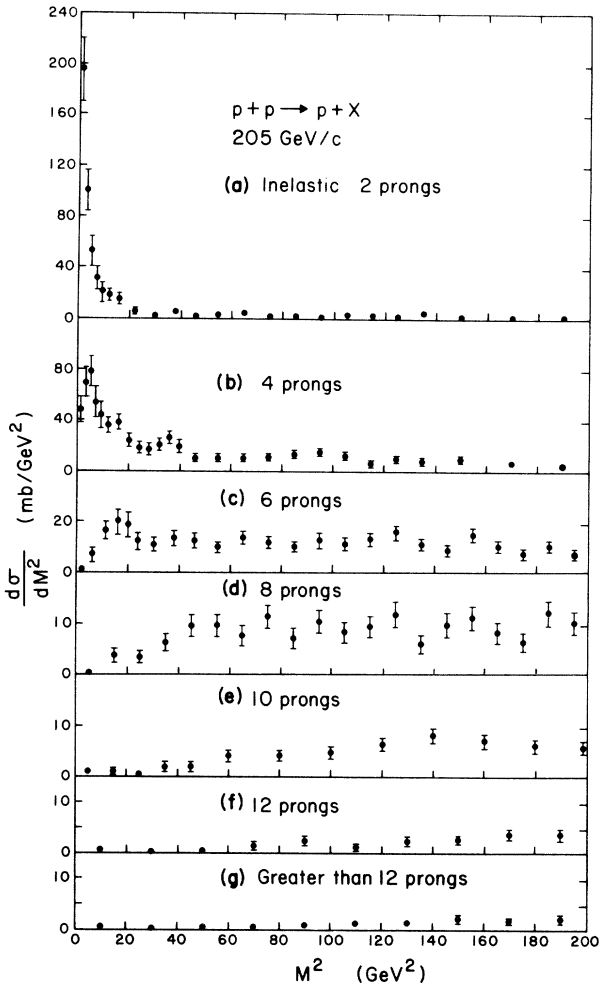

FIG. 10. $d\sigma/dM^2$ for different charged multiplicities.

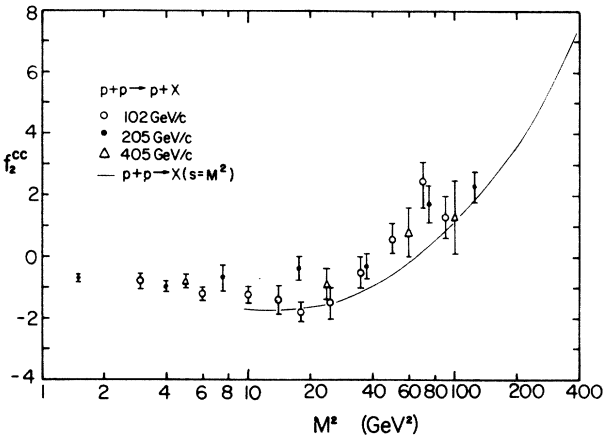

FIG. 11. Mueller parameter $f_2^{cc} = \langle n_c(n_c - 1)\rangle - \langle n_c\rangle^2$ for the reaction $p + p \to p + X$ as a function of M^2. The solid line represents data from $p + p \to X$ as a function of $s = M^2$.

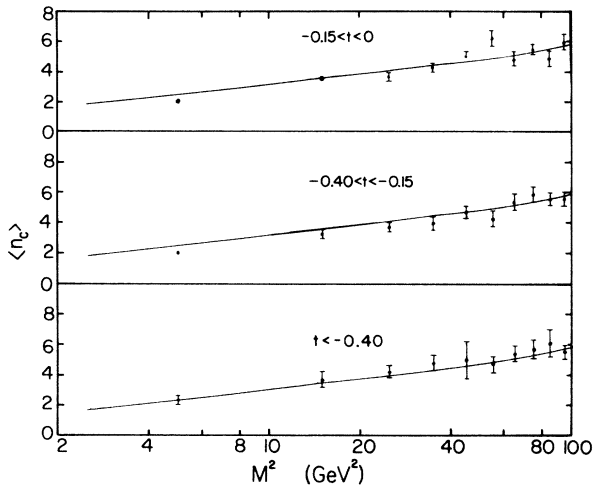

FIG. 12. Average charged multiplicity, $\langle n_c \rangle$, as a function of M^2 for different t values. The solid line represents the dependence after integration over all t.

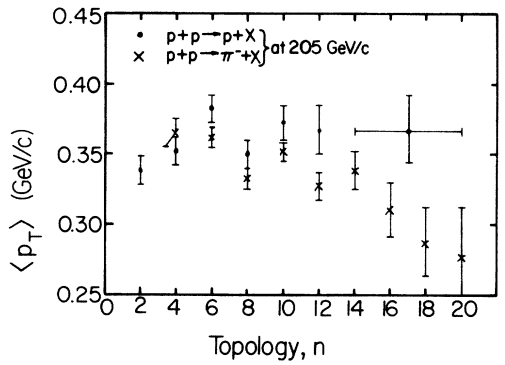

FIG. 14. Average value of the transverse momentum, $\langle p_T \rangle$, for protons and π^- as a function of the final-state charged-particle multiplicity, n.

obtained after integration over all t (see Ref. 6). We note that the M^2 dependence is consistent with being independent of t. Another way to see this is shown in Fig. 13 which presents $\langle n_c \rangle$ as a function of p_T for different values of M^2. For values of $p_T \lesssim 0.9$ GeV/c, we see no dependence of the average multiplicity on p_T. This does not conflict with data from BNL[17] which indicate that a rise in $\langle n \rangle$ occurs for $p_T \gtrsim 1$ GeV/c. In our experiment we are unable to measure transverse momenta greater than ~1 GeV/c due to (a) the laboratory momentum cut of 1.4 GeV/c, and (b) a lack of statistics since

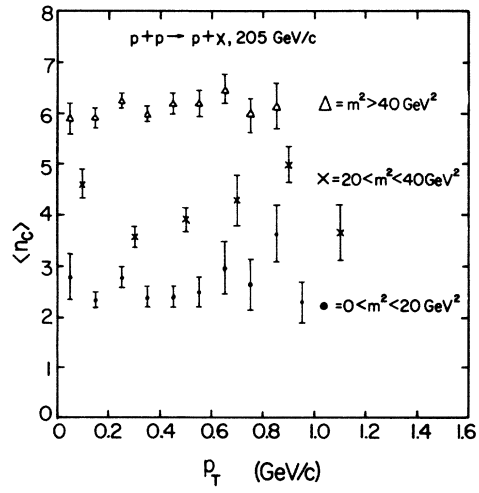

FIG. 13. Average charged multiplicity, $\langle n_c \rangle$, as a function of p_T for different M^2 values.

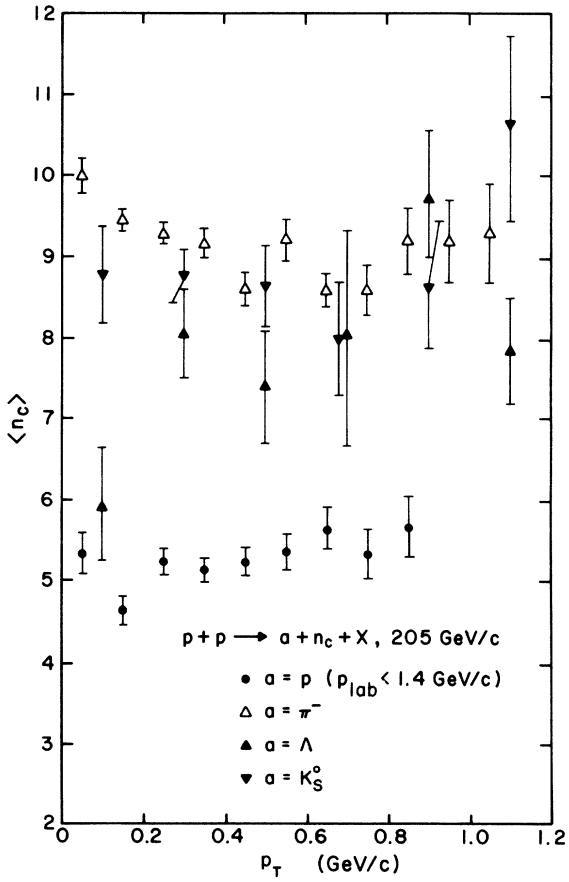

FIG. 15. Average charged multiplicity associated with the production of different kinds of particles as a function of p_T.

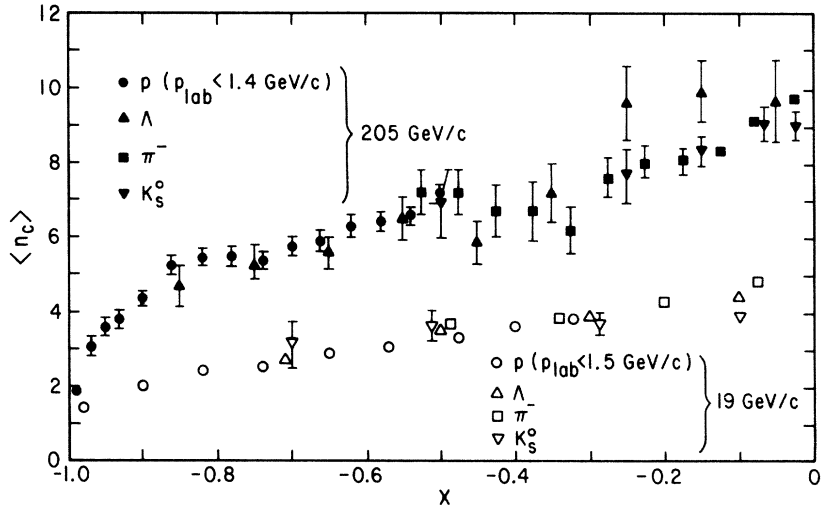

FIG. 16. Average charged multiplicity associated with the production of different kinds of particles as a function of $x = 2p_L^*/\sqrt{s}$ for 205-GeV/c and 19-GeV/c pp interactions.

the cross sections are falling approximately exponentially in p_T^2.

Figure 14 shows the average value of the transverse momentum of the proton, $\langle p_T \rangle$, as a function of the final-state charged multiplicity, n. There is, perhaps, an indication that the higher multiplicities are associated with higher transverse momentum protons, in contrast to inclusive π^- production which indicates that $\langle p_T(\pi^-) \rangle$ decreases as a function of n.[18]

Finally, in Figs. 15 and 16 we compare the average charged multiplicities associated with a slow proton to those observed in association with other kinds of particles. Figure 15 shows $\langle n_c \rangle$ as a function of p_T for events associated with a proton, K_S^0, Λ, and π^- from 205 GeV/c pp interactions.[18,19] This figure shows the same effect as observed in 19 GeV/c pp interactions,[20] namely, that slow protons tend to be associated with lower charged multiplicity events than K_S^0, Λ, or π's.

Figure 16 shows, however, that the differences observed in Fig. 15 are associated with the fact that different kinds of particles populate different regions of phase space. If one picks a selected region in phase space, as characterized by x, then Fig. 16 indicates that the observed charged multiplicity associated with a given kind of particle depends primarily not on the intrinsic properties of the particle itself but rather on the x value of the produced particle. A similar result[20] has been found at 19 GeV/c and is also shown in Fig. 16.

V. CONCLUSIONS

In this paper we have presented inclusive distributions for proton production in pp interactions at 205 GeV/c. The invariant cross sections reported here cover wider ranges in the variables t and M^2 than have been obtained in counter experiments at either the ISR or Fermilab. We hope that these data will be useful for analyses in the triple Regge model[21] both for the charged multiplicity dependence as well as for the inclusive production cross section dependence on kinematic variables.

ACKNOWLEDGMENTS

We gratefully acknowledge the help of the 30-in. bubble-chamber crew and members of the Fermilab Neutrino Laboratory staff during the running of this experiment. We thank the Argonne National Laboratory scanning and measuring staff for their efforts.

---

*Present address: Michigan State University, East Lansing, Michigan 48823.
†Operated by Universities Research Association, Inc. under contract with the United States Atomic Energy Commission.
‡On leave from the University of Birmingham, Birmingham, England.
§Work supported by the United States Atomic Energy Commission.
[1] M. G. Albrow *et al.*, Nucl. Phys. B51, 388 (1973); B54, 6 (1973).
[2] F. Sannes *et al.*, Phys. Rev. Lett. 30, 766 (1973);

K. Abe *et al.*, *ibid.* 31, 1527 (1973); 31, 1530 (1973).
[3]S. Childress *et al.*, Phys. Rev. Lett. 32, 389 (1974).
[4]J. W. Chapman *et al.*, Phys. Rev. Lett. 32, 257 (1974).
[5]F. T. Dao *et al.*, Phys. Lett. 45B, 399 (1973); *Experiments on High Energy Particle Collisions—1973*, proceedings of the International Conference on New Results from Experiments on High Energy Particle Collisions, Vanderbilt University, 1973, edited by Robert S. Panvini (A.I.P., New York, 1973), p. 36.
[6]S. J. Barish *et al.*, Phys. Rev. Lett. 31, 1080 (1973).
[7]J. Whitmore and M. Derrick, Phys. Lett. 50B, 280 (1974).
[8]S. Barish *et al.*, Phys. Rev. D 9, 2689 (1974).
[9]For details of the separation of elastic and inelastic events, see S. Barish *et al.*, Phys. Rev. D 9, 1171 (1974), and footnote 6 of Ref. 6.
[10]We thank J. Vander Velde for discussions on this point.
[11]The 19 GeV/c data are from the Scandinavian collaboration, private communication from H. Bøggild. The 28.5-GeV/c data are from the BNL-Vanderbilt Collaboration, private communication from J. Hanlon.
[12]For a summary of the Fermilab bubble-chamber data, see J. Whitmore, Phys. Rep. 10C, 273 (1974).
[13]H. Bøggild *et al.*, Nucl. Phys. B27, 285 (1971).
[14]M. Antinucci *et al.*, Nuovo Cimento Lett. 6, 121 (1973).
[15]F. Winkelmann, Phys. Lett. 48B, 273 (1974).
[16]C. Bromberg and T. Ferbel (private communication).
[17]A. Ramanauskas *et al.*, Phys. Rev. Lett. 31, 1371 (1973).
[18]R. Singer (private communication).
[19]K. Jaeger (private communication).
[20]H. Bøggild *et al.*, Nucl. Phys. B72, 221 (1974).
[21]Two recent triple-Regge analyses that use these data are D. P. Roy and R. G. Roberts, Nucl. Phys. B77, 240 (1974); R. D. Field and G. C. Fox, *ibid.* B80, 367 (1974).